Journal of Manufacturing Systems 46 (2018) 247–263

Contents lists available at ScienceDirect

Journal of Manufacturing Systems

journal homepage: www.elsevier.com/locate/jmansys

A fast and adaptive bi-dimensional empirical mode decomposition approach for filtering of workpiece surfaces using high definition metrology

Shichang Du [a,b,*], Tao Liu [a], Delin Huang [a], Guilong Li [a]

[a] School of Mechanical Engineering, Shanghai Jiaotong University, Shanghai, 200240, China
[b] State Key Lab of Mechanical System and Vibration, Shanghai Jiaotong University, Shanghai, 200240, China

ARTICLE INFO

Article history:
Received 9 October 2017
Received in revised form 5 January 2018
Accepted 6 January 2018
Available online 24 January 2018

Keywords:
Workpiece surface quality
Filtering
High definition metrology
Bi-dimensional empirical mode decomposition
Surface topography analysis

ABSTRACT

The surface topography of workpieces has an important influence on the final performances of the product. The digital filtering is a critical step to analyze the surface topography of workpieces. Bi-dimensional empirical mode decomposition (BEMD) approach is superior to conventional filtering approaches in the analysis of non-stationary and non-linear data. High definition metrology (HDM) can generate massive point cloud data to represent the three-dimensional (3D) surface topography of workpieces, which provides a new opportunity for surface topography analysis. This paper develops a fast and adaptive bi-dimensional empirical mode decomposition (FABEMD) approach for filtering of workpiece surfaces using HDM. Firstly, the neighboring window algorithm is presented to extract local extrema and draw the extrema spectrum. Secondly, the adaptive window algorithm is developed to automatically select the optimal window size of the order statistics filter, and plot the envelope spectrum. Finally, the average smoothing filter is presented for smooth filtering and generating of the mean envelope. The performance of the proposed FABEMD-based filter is validated by a simulated surface data and three real-world surface data. Compared with Gaussian filter (ISO 11562:1996, ASME B46.1-2002), the BEMD-based filter and the recent shearlet-based filter in the qualitative and quantitative analysis, the proposed FABEMD-based filter is superior for the separation and extraction of different surface components.

1. Introduction

The surface texture is an important index to evaluate the quality of workpieces [1,2], and is generally described from the small to the large scale: roughness, waviness and form. It is well-known that different components of the surface texture have different influences on the functional performance of workpieces. To be specific, roughness is a good indicator of the surface irregularities, thus can be applied to detect errors in the material removal process, and also it has great influence on the workpiece functionality such as wear and friction. Waviness, which may occur from machine or work deflections, chatter, residual stress, vibrations, or heat treatment, has influence on tightness of workpieces. Form may directly affect the assembling performance of workpieces. Therefore, the motivation for separating these components derives from the fact that they have different origins and influences on workpieces functionalities in different ways. It is very important to separate the surface texture into different components before surface topography analysis.

Digital filtering is an essential step to realize the separation process. Filtering of workpiece surfaces has been a hot research topic on account of its importance for surface texture analysis. The traditional filtering approaches such as 2RC filter and Gaussian filter have been firstly studied, and the Gaussian filter is one of the most widely-used standard filtering approaches. However, it is well recognized that it is not robust against outliers. To overcome the shortcoming, some modified approaches such as robust regression Gaussian filter [3], spline filter [4], robust spline filter [5], and morphological filter [6] have been developed. Recent advances in filtering approaches are reviewed in [7,8].

Several researchers develop wavelet-based filtering approaches and apply them to analyze workpiece surfaces. Different from the previous filtering approaches, wavelet-based filters can provide multi-scale analysis since they can divide a surface profile into different frequency components and investigate each component with a resolution matched to its scale. Fu et al. [9]

* Corresponding author at: School of Mechanical Engineering, Shanghai Jiaotong University, Shanghai, 200240, China.
E-mail addresses: lovbin@sjtu.edu.cn (S. Du), l_yz2007@163.com (T. Liu), cjwanan@sjtu.edu.cn (D. Huang), lgl52613@sjtu.edu.cn (G. Li).

https://doi.org/10.1016/j.jmsy.2018.01.005
0278-6125/

adopted the wavelet transform to surface topography analysis and compared different wavelet bases. Orthogonal wavelet bases and biorthogonal wavelet bases were recommended due to their transmission characteristics of the corresponding filters. Jiang et al. [10] proposed a lifting wavelet representation for characterization of surface topography. Josso et al. [11] proposed a frequency normalized wavelet transform for surface roughness analysis and characterization. Wang et al. [12] proposed a modified anisotropic diffusion filter to separate workpiece surfaces into various scale-limited surfaces. Most recently, Du, Liu and Huang [13] presented a shearlet-based filtering approach. The workpiece surface was decomposed into different sub-bands of coefficients with non-subsampled shearlet transform (NSST). Then the surface components at different level were reconstructed based on inverse NSST.

Recently, Huang et al. [14] and Du et al. [15] introduced and improved the empirical mode decomposition (EMD) approach to analyze one-dimensional non-stationary and non-linear signals based on instantaneous frequency. Flandrin [16] proposed the concept of filter banks based on EMD and the corresponding order intrinsic mode functions (IMFs) were combined to achieve the high-pass, low-pass and band-pass filters. Wu and Huang [17] confirmed that the EMD approach had similar filtering characteristics with the wavelet-based approaches. Boudraa and Cexus [18] used different thresholds for each IMF to reconstruct the new filter and realize the signal denoising. Nevertheless, EMD cannot be used to analyze 3D data.

Nunes [19] proposed a bi-dimensional EMD (BEMD) appraoch, which is a two-dimensional (2D) extension of the EMD approach, mainly used for image processing [20], image denoising [21], image edge pattern processing [22] and medical image registration [23], not used for filtering of workpiece surfaces. Moreover, since the window size of order statistic filters in the BEMD approach is not determined adaptively, it frequently does not have the best filtering results. Bhuiyan [24,25] proposed a fast and adaptive BEMD (FABEMD) approach. Simulation results demonstrate that FABEMD is not only faster and adaptive, but also outperforms the original BEMD in terms of the quality of the BIMFs.

With the development of on-line high definition measurement (HDM) technologies, great opportunities are provided for on-line controlling surface quality. A representative of on-line HDM for surface variation measurement is Shapix based on laser holographic interferometry metrology [26], which measures 3D surface height map and gains millions of data points within seconds, and has 150 μm resolution in x–y direction and 1 μm accuracy in z direction. Based on HDM, some researches about surface quality control and engineering applications have been successfully conducted, such as surface classification [27,28], tool wear monitoring [29], form error evaluation and estimation [30,31], volume variation control [32], and flat surface variation control [33]. However, to the best knowledge of the authors, there is no BEMD-based filtering approach for workpiece surfaces using HDM. The high density point cloud data of HDM is large. About one million measurement points are collected from a cylinder head by HDM system. So, HDM needs a fast and adaptive analysis. Therefore, this paper presents a novel fast and adaptive bi-dimensional empirical mode decomposition (FABEMD) approach for filtering of workpiece surfaces using HDM.

The remainder of this paper is organized as follows: The BEMD approach is briefly introduced in Section 2. In Section 3, the proposed approach of filtering workpiece surfaces is presented. In Section 4, a simulation experiment is conducted to validate the feasibility of the presented approach. In Section 5, three case studies using different kinds of workpiece surfaces are presented to show the effectiveness of the proposed approach. In Section 6, the conclusions of this study are drawn.

2. Brief introduction to BEMD

The BEMD approach decomposes a signal into its bi-dimensional IMFs (BIMFs) and a residue based on the local spatial scales. Let the original signal be denoted as $I(x, y)$, a BIMF as $F(x, y)$, and the residue as $R(x, y)$. The original bi-dimensional signal $I(x, y)$ can be decomposed by BEMD

$$I(x,y)=\sum F_i(x,y)+R(x,y) \tag{1}$$

where $F_i(x, y)$ is the i-th BIMF obtained from its source signal $S_i(x, y)$, and $S_i(x, y) = S_{i-1}(x, y) - R_{i-1}(x, y)$.

It requires one iteration or more to obtain $F_i(x, y)$, and the intermediate state of a BIMF in j-th iteration can be denoted as $F_{Tj}(x, y)$. The decomposition steps of the BEMD approach are summarized as follow:

Step 1: Set $i = 1$ and $S_i(x, y) = I(x, y)$.

Step 2: Set $j = 1$ and $ST_j(x, y) = S_i(x, y)$. ST_j represents the input signal of the jth decomposition.

Step 3: Obtain the local maxima map of $F_{Tj}(x, y)$, denoted as $P_j(x, y)$.

Step 4: Interpolate the maxima points in $P_i(x, y)$ and generate the upper envelope, denoted as $U_{Ej}(x, y)$.

Step 5: Obtain the local minima map of $F_{Tj}(x, y)$, denoted as $Q_j(x, y)$.

Step 6: Interpolate the minima points in $Q_i(x, y)$and generate the lower envelope, denoted as $L_{Ej}(x, y)$.

Step 7: Calculate the mean envelope $M_{Ej}(x, y) = (U_{Ej}(x, y) + L_{Ej}(x, y))/2$.

Step 8: Calculate the details of the signal in the decomposition process,$F_{Tj+1}(x, y) = F_{Tj}(x, y) - M_{Ej}(x, y)$.

Step 9: Check whether $F_{Tj+1}(x, y)$ follows the BIMF properties by finding the standard deviation (SD), denoted as D (Eq. (2)), between $F_{Tj+1}(x, y)$and $F_{Tj}(x, y)$, and compare it with the desired threshold.

$$D=\sum_{x=1}^{M}\sum_{j=1}^{N}\frac{\left|F_{Tj+1}(x,y)-F_{Tj}(x,y)\right|^{2}}{\left|F_{Tj}(x,y)\right|^{2}} \tag{2}$$

where (x, y) is the coordinate, M is the total number of rows and N is the total number of columns of the 2D data. The value of D is usually chosen to be 0.5 to ensure that the mean value of BIMF is close to 0.

Step 10: If $F_{Tj+1}(x, y)$ meets the criteria according to step 9, then $F_j(x, y) = F_{Tj+1}(x, y)$, set $S_{i+1}(x, y) = S_i(x, y)$ and $i = i + 1$, and go to step 11. Otherwise set $j = j + 1$, go to step 3 and continue up to step 10.

Step 11: Determine whether $S_i(x, y)$ has less than three extrema points, and if so, the residual $R(x, y) = S_i(x, y)$, and the decomposition is complete. Otherwise, go to step 2 and continue up to step 11.

In the process of extracting BIMFs, the number of extreme points in $S_{i+1}(x, y)$ should be less than the number of extreme points in $S_i(x, y)$. Let the BIMFs and the residual of a signal together be named as bi-dimensional empirical mode components (BEMCs). All the BEMCs compose the original 2D signal as follow

$$\sum F(x,y)=\sum_{i=1}^{K+1}F_i(x,y)=I(x,y) \tag{3}$$

where $F_i(x, y)$ is the i-th BEMC, and K is the total number of BEMCs except the residual.

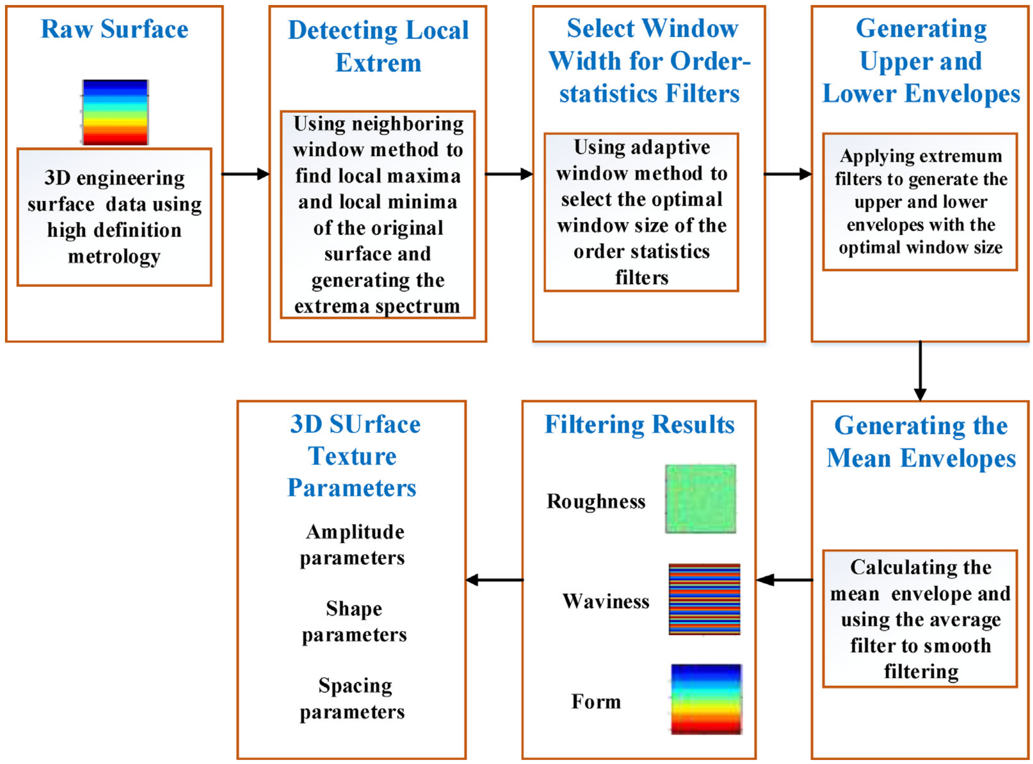

Fig. 1. The framework of the proposed approach.

3. The proposed approach

3.1. Overview of the proposed approach

This section proposes an FABEMD approach for filtering of workpiece surfaces using HDM. Compared with the original BEMD approach, three aspects are improved: 1) The proposed approach does not need to calculate the minimum Euclidean distance between adjacent extreme points and does not need to calculate adjacent maxima and minima distance array. 2) The proposed approach uses the adaptive window algorithm to optimally select the window size of the order statistics filters. 3) The envelope surface is drawn by the extremum filters and the average filters, so the computation time is greatly saved.

The framework of the proposed approach is shown in Fig. 1, and the procedure involves the following steps.

Step 1: Read the 3D engineering surface data collected by HDM.

Step 2: Use the neighboring window algorithm to find local maxima and local minima of the original surface, and generate the extrema spectrum.

Step 3: Use the developed adaptive window algorithm to select the optimal window size of the order statistics filters.

Step 4: Apply extremum filters to generate the upper and lower envelopes with the optimal window size.

Step 5: Calculate the mean envelope and use the average filter to smooth filtering.

Step 6: Decompose into roughness, waviness and form.

Step 7: Calculate the 3D surface parameters of the decomposed components, amplitude parameters, shape parameters and spacing parameters for surface texture analysis.

3.2. Detecting local extrema

In detection of local extrema, the local maxima and minima points from the given data need to be found. The 2D array of local maxima (minima) points is called a maxima (minima) map. This paper uses the neighboring window algorithm to find local maxima points P_{ij} and local minima points Q_{ij}. In this algorithm, a data point is considered as a local maximum (minimum), if its value is strictly higher (lower) than all of its neighbors. Let $A(x, y)$ be an $M \times N$ 2D matrix represented by

$$A(x,y) = \begin{bmatrix} a_{11} & a_{12} & \cdots & a_{1N} \\ a_{21} & a_{22} & \cdots & a_{2N} \\ \vdots & \vdots & \cdots & \vdots \\ a_{M1} & a_{M2} & \cdots & a_{MN} \end{bmatrix} \quad (4)$$

where a_{mn} is the element of $A(x, y)$ located in the m-th row and n-th column.

Let the window size for local extrema determination be $w_{ex} \times w_{ex}$. Then, the extrema points are calculated by

$$a_{mn} \triangleq \text{Local Maximum}, \ \text{if}\, a_{mn} > a_{kl}; \quad \text{Local Minimum}, \text{if}\, a_{mn} < a_{kl}; \quad (5)$$

where

(6)

Generally, a given 2D data only needs a 3×3 window to get an optimum extrema map. A higher window size may result in a lower number of local extrema points for a given data matrix. In order to find extrema points at the boundary or corner, the neighboring points within the window that are beyond the boundary are neglected. For illustration purposes, consider an 8×8 matrix given in Fig. 2(a). The maxima map given in Fig. 2(b) and minima map given in Fig. 2(c) are obtained through applying a 3×3 neighboring window for every point in the matrix.

8	9	4	1	5	2	6	3
6	3	2	3	8	3	9	3
7	8	3	4	1	4	3	7
3	1	2	4	3	5	7	8
7	4	2	1	2	5	3	4
1	3	7	9	9	8	7	8
9	2	6	7	6	8	7	7
8	2	1	9	7	9	1	1

(a) A sample 8×8 matrix

0	9	0	0	0	0	0	0
0	0	0	0	8	0	9	0
0	8	0	0	0	0	0	0
0	0	0	0	0	0	0	8
7	0	0	0	0	0	0	0
0	0	0	0	0	0	0	8
9	0	0	0	0	0	0	0
0	0	0	9	0	9	0	0

(b) local maxima map obtained from (a)

0	0	0	1	0	2	0	0
0	0	0	0	0	0	0	0
0	0	0	0	1	0	0	0
0	1	0	0	0	0	0	0
0	0	0	1	0	0	3	0
1	0	0	0	0	0	0	0
0	0	0	0	6	0	0	0
0	0	1	0	0	0	0	0

(c) local minima map obtained from (a)

Fig. 2. A sample 8 × 8 data matrix using the neighboring window algorithm.

3.3. Adaptive window algorithm to select window width for order-statistics filters

After obtaining the extrema map, the next step is to draw the upper and lower envelope. The core of the traditional BEMD approach is the order statistics filter, in which the maximum value filter (MAX Filter) is used to draw the upper envelope, and the minimum value filter (MIN Filter) is used to draw the lower envelope. Order statistics filters are spatial filters whose responses are determined based on ordering (ranking) the elements contained within the data area encompassed by the filters. The response of the filters at any point is determined by the ranking result. For the envelope estimation approach, the most important part is the order statistics filter, and for the order statistics filter, the crucial part is to select an appropriate window size for the filter.

There are four types of the window sizes ($d_1 \le d_2 \le d_3 \le d_4$) for an order statistic filter determined by the extrema spectrum (Eq. (7)).

$$\begin{aligned} w_{en} &= \mathrm{d}_1 = \mathrm{minimum}\{\mathrm{minimum}\{\mathrm{d}_{\text{adj-max}}\},\ \mathrm{minimum}\{\mathrm{d}_{\text{adj-min}}\}\} \\ w_{en} &= \mathrm{d}_2 = \mathrm{max\,imum}\{\mathrm{minimum}\{\mathrm{d}_{\text{adj-max}}\},\ \mathrm{minimum}\{\mathrm{d}_{\text{adj-min}}\}\} \\ w_{en} &= \mathrm{d}_3 = \mathrm{min\,imum}\{\mathrm{maximum}\{\mathrm{d}_{\text{adj-max}}\},\ \mathrm{max\,imum}\{\mathrm{d}_{\text{adj-min}}\}\} \\ w_{en} &= \mathrm{d}_4 = \mathrm{max\,imum}\{\mathrm{maximum}\{\mathrm{d}_{\text{adj-max}}\},\ \mathrm{max\,imum}\{\mathrm{d}_{\text{adj-min}}\}\} \end{aligned} \tag{7}$$

where w_{en} is the window size of an order statistic filter, $\mathrm{d}_{adj-max}$is adjacent maxima distance array and d is adjacent minima distance array.

There is always an optimal window size of an order statistic filter in the interval $[d_1, d_4]$ for a workpiece surface, which makes the FABEMD approach have the best filtering results. It is usually difficult to adaptively choose an optimal window size for a workpiece surface. Therefore, an adaptive window algorithm is developed to automatically select the optimal window size of order statistics filters. The flow chart of the proposed adaptive window algorithm is shown in Fig. 3, and the specific implementation process is described as follows.

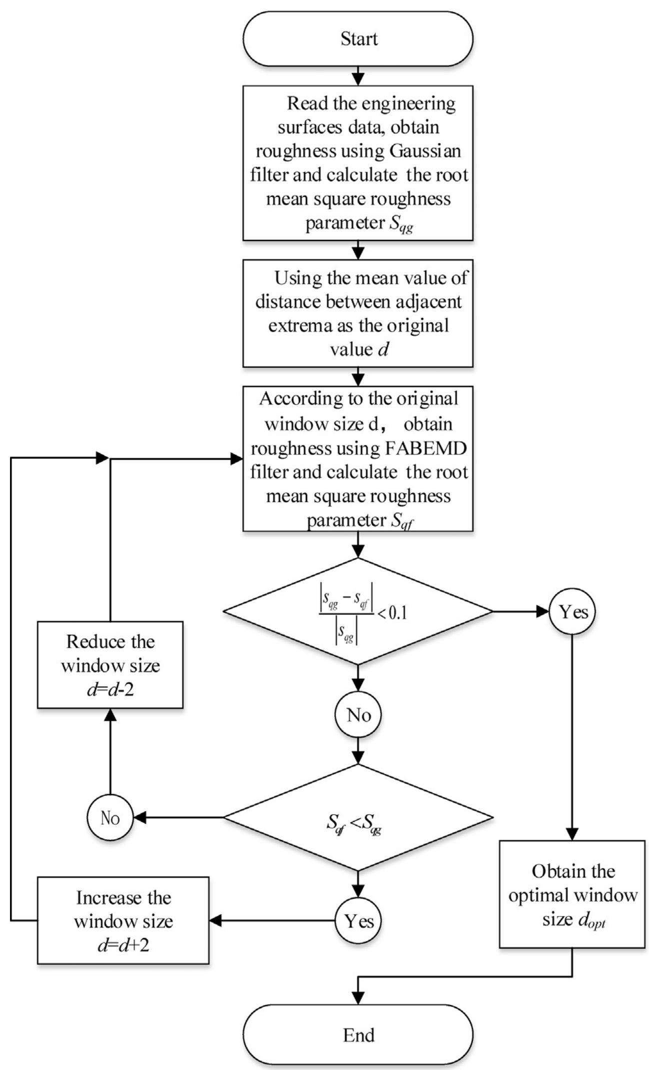

Fig. 3. Flow chart of the adaptive window algorithm.

Step 1: Read the workpiece surfaces data, obtain roughness using Gaussian filter and calculate the root mean square roughness parameter S_{qg} as the reference value.

$$S_{qg} = \sqrt{\frac{1}{A}\iint_A z^2(x, y)\,\mathrm{d}x\mathrm{d}y} \tag{8}$$

Step 2: Calculate the window size d of order statistics filters and the original window size d as shown in Eq. (9).

$$d = \frac{1}{2} \times \sqrt{\frac{M \times N}{n_{extrem}}} \tag{9}$$

where $M \times N$ is the image size, and n_{extrem} is the sum of the numbers of localized maxima and minima. A value of d corresponds to the distance between extrema in case of its uniform distribution.

$$S_{qf} = \sqrt{\frac{1}{A}\iint_A z^2(x, y)\,\mathrm{d}x\mathrm{d}y} \tag{10}$$

9	9	9	8	8	9	9	9
9	9	9	8	8	9	9	9
8	8	8	8	8	9	9	9
8	8	8	4	5	7	8	8
7	7	9	9	9	9	8	8
9	9	9	9	9	9	8	8
9	9	9	9	9	9	9	8
9	9	9	9	9	9	9	7

(a) upper envelope matrix using maximum filter before smoothing

3	2	1	1	1	2	2	3
3	2	1	1	1	1	2	3
1	1	1	1	1	1	3	3
1	1	1	1	1	1	3	3
1	1	1	1	1	2	3	3
1	1	1	1	1	2	3	3
1	1	1	1	6	1	1	1
2	1	1	1	6	1	1	1

(b) lower envelope matrix using minimum before smoothing

Fig. 4. The upper and lower envelope matrix using maximum filter and minimum filter before smoothing.

Step 3: According to the original window size d, obtain workpiece surface roughness using FABEMD filter and calculate the root mean square roughness parameter S_{qf}.

Step 4: Calculate the deviation ratio δ (Eq. (11)). When $\delta < 0.1$, go to step 6, otherwise, go to step 5.

$$\delta = \frac{|S_{qg} - S_{qf}|}{|S_{qg}|} \times 100\% \tag{11}$$

Step 5: If $S_{qf} < S_{qg}$, then increase the window size of order statistics filters, set $d = d + 2$, and return to step 3 until $\delta < 0.1$. If $S_{qf} > S_{qg}$, reduce the window size of order statistics filters, set $d = d - 2$, and return to step 3 until $\delta < 0.1$.

Step 6: If $\delta < 0.1$, stop searching, obtain the optimal window size d_{opt}, and the program ends.

3.4. Generating envelopes

After determining the optimal window size of order statistics filter for envelope information, the maximum and minimum filters are applied to obtain the upper and lower envelopes, UE_{ij} and LE_{ij} respectively

$$UE_{ij}(x, y) = \underset{(s,t) \in Z_{xy})}{\mathrm{MAX}} \left\{ S_{ij}(s, t) \right\} \tag{12}$$

$$LE_{ij}(x, y) = \underset{(s,t) \in Z_{xy})}{\mathrm{MIN}} \left\{ S_{ij}(s, t) \right\} \tag{13}$$

In Eq. (12), the value of the upper envelope UE_{ij} at any point (x, y) is the maximum value of the elements in S_{ij} in the region defined by Z_{xy}. Z_{xy} is the square region of size $W_{en} \times W_{en}(W_{en} = d_{opt})$ centered at any point (x, y) of S_{ij}. Similarly, the value of the lower envelope LE_{ij} at any point (x, y) is the minimum value of the elements in S_{ij} in the region defined by Z_{xy} in Eq. (13). It should be noted that the maximum filter and minimum filter produce new 2D matrices for upper and lower envelope surfaces from the given 2D data matrix, and they do not alter the actual 2D data. Since smooth continuous surfaces for upper and lower envelopes are preferable, averaging smoothing operations are carried out on both UE_{ij} and LE_{ij} by applying the same window size for corresponding order statistics filters. The averaging smoothing operations are expressed as

$$UE_{ij}(x, y) = \frac{1}{w_{sm} \times w_{sm}} \sum_{(s,t) \in Z_{xy}} UE_{ij}(s, t) \tag{14}$$

$$LE_{ij}(x, y) = \frac{1}{w_{sm} \times w_{sm}} \sum_{(s,t) \in Z_{xy}} LE_{ij}(s, t) \tag{15}$$

where Z_{xy} is the square region of size $W_{sm} \times W_{sm}$ centered at any point (x, y) of UE_{ij} or LE_{ij}, W_{sm} is the window width of the averaging smoothing filter and $W_{sm} = W_{en} = d_{opt}$.

The operation in Eq. (14) is the arithmetic mean filtering. From the smoothed envelopes UE_{ij} and LE_{ij}, the mean or average envelope ME_{ij} is calculated as

$$ME_{ij} = (UE_{ij} + LE_{ij})/2 \tag{16}$$

A 3×3 window for maximum and minimum filters is applied to the data matrix of Fig. 2(a), and the results in the upper and lower envelope matrices are shown in Fig. 4(a) and (b), respectively. Window width W_{en} obtained by Type-3 is 3. The averaging smoothing operations are applied to Fig. 4(a) and (b), and the results in the smoothed upper and lower envelope matrices are shown in Fig. 5(a) and (b), respectively. The mean envelope matrix produced by averaging the matrices of Fig. 5(a) and (b) is shown in Fig. 5(c) according to Eq. (16).

In the BEMD approach, SD criterion (Eq. (2)) is employed as the most important stopping criterion, and the maximum number of allowable iterations is used as an auxiliary stopping criterion to prevent the occurrence of over-sifting.

The correlation coefficient is used to evaluate the similarity between two vectors.

$$r = \frac{\sum_m \sum_n (A_{mn} - \bar{A})(B_{mn} - \bar{B})}{\sqrt{\left(\sum_m \sum_n (A_{mn} - \bar{A})^2 \right) \left(\sum_m \sum_n (B_{mn} - \bar{B})^2 \right)}} \tag{17}$$

where r is utilized to evaluate the correlation coefficient of the matrixes or vectors with the same size. $\bar{A}(\bar{B})$ is the mean value of A (B). The number of rows and columns of A and B is M and N, respectively. The larger the correlation coefficient is, the bigger the similarity is. Conversely, the smaller the correlation coefficient is, the smaller the similarity is.

4. Simulation experiment

To verify the performance of the proposed approach, a simulated 3D surface is randomly generated and filtered using the proposed FABEMD approach. Then, the filtering result is compared with the original BEMD approach. The size of the simulated surface is 42 mm × 42 mm, the sampling interval is 0.1 mm, and the numerical expression of the surface is described as follows.

$$z(x, y) = 0.8 \times x + 0.8 \times \sin(0.4 \times \pi \times y) + 0.5 \times \mathrm{normrnd}(0, 0.1) 0 \le x \le 42\mathrm{mm}, 0 \le y \le 42\mathrm{mm} \tag{18}$$

where normrnd (μ, δ) denotes random number following the normal distribution with mean parameter $\mu = 0$ and standard deviation parameter $\delta = 0.1$. $0.5 \times$ normrnd(0, 0.1)(a random noise) is the

9.0	9.0	8.7	8.3	8.3	8.7	9.0	9.0
8.7	8.7	8.4	8.2	8.3	8.7	9.0	9.0
8.3	8.3	7.8	7.3	7.3	8.0	8.6	8.7
7.7	7.9	7.7	7.6	7.6	8.0	8.3	8.3
8.0	8.2	8.0	7.9	7.8	8.0	8.1	8.0
8.3	8.6	8.8	9.0	9.0	8.8	8.4	8.2
9.0	9.0	9.0	9.0	9.0	8.9	8.4	8.2
9.0	9.0	9.0	9.0	9.0	9.0	8.5	8.3

(a) upper envelope matrix after smoothing

2.5	2.0	1.3	1.0	1.2	1.5	2.2	2.5
2.0	1.7	1.2	1.0	1.1	1.6	2.2	2.7
1.5	1.3	1.1	1.0	1.0	1.6	2.2	2.8
1.0	1.0	1.0	1.0	1.1	1.8	2.4	3.0
1.0	1.0	1.0	1.0	1.2	1.9	2.6	3.0
1.0	1.0	1.0	1.6	1.8	2.2	2.1	2.3
1.2	1.1	1.0	2.1	2.2	2.4	1.6	1.7
1.3	1.2	1.0	2.7	2.7	2.7	1.0	1.0

(b) lower envelope matrix after smoothing

5.8	5.5	5.0	4.7	4.8	5.1	5.6	5.8
5.3	5.2	4.8	4.6	4.7	5.1	5.6	5.8
4.9	4.8	4.4	4.2	4.2	4.8	5.4	5.8
4.3	4.4	4.3	4.3	4.3	4.9	5.4	5.7
4.5	4.6	4.5	4.4	4.5	4.9	5.3	5.5
4.7	4.8	4.9	5.3	5.4	5.5	5.3	5.3
5.1	5.1	5.0	5.6	5.6	5.7	5.0	4.9
5.1	5.1	5.0	5.8	5.8	5.8	4.8	4.6

(c) mean envelope matrix obtained by averaging the data in (a) and (b)

Fig. 5. The envelope matrix after smoothing.

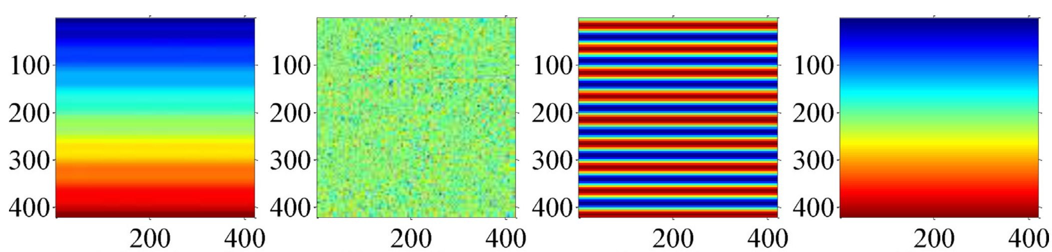

(a) Original profile (b) Roughness (c) Waviness (d) Form

Fig. 6. Simulated surface and its components.

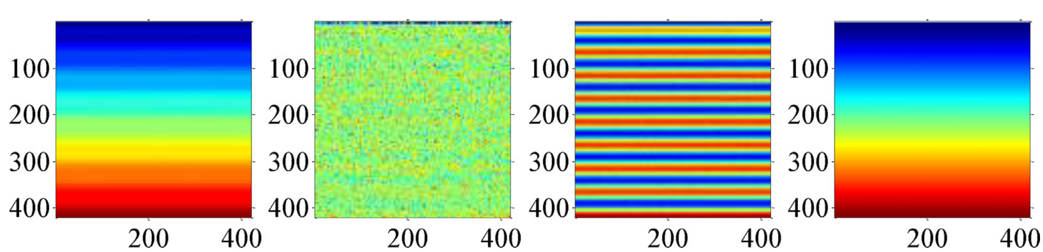

(a) Synthetic surface (b) Roughness (c) Waviness (d) Form

Fig. 7. Filtering result of simulated surface using the proposed FABEMD approach.

roughness component, $0.8 \times \sin(0.4 \times \pi \times y)$ (a sinusoidal function) is the waviness component and $0.8 \times x$(an inclined surface) is the form component. The simulated surface and its components are shown in Fig. 6.

Fig. 7 shows the filtering results using the FABEMD approach to the simulated surface. From Fig. 7, it can be seen that Figs. 6(b)–(d) and 7(b)–(d) have obvious similarity. The correlation coefficients of Figs. 6(b)–(d) and 7(b)–(d) are 0.9423, 0.9701 and 0.9997 respectively. Therefore, the proposed FABEMD approach can properly separate the simulated surface into different surface components and can effectively eliminate mode mixing.

The simulated surface is decomposed by the original BEMD approach and the decomposition results are shown in Fig. 8. From Fig. 8, it can be seen that two sets of BIMF components (BIMF1 and BIMF2, BIMF3 and BIMF4) have a similar scale and mutual influence. According to Eq. (17), the correlation coefficients of BIMF1 and BIMF2, BIMF3 and BIMF4 are 0.9349 and 0.7596 respectively. The three simulated components cannot be separated into different BIMFs, and the mode mixing problem occurs.

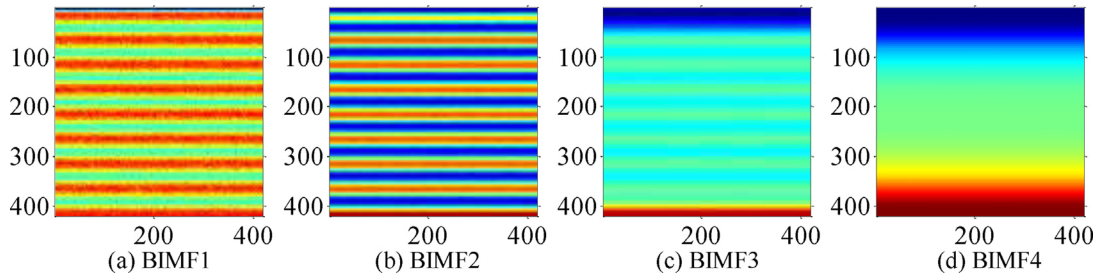

Fig. 8. Filtering result of simulated surface using the original BEMD approach.

5. Case studies

In order to further validate the effectiveness of the proposed approach, the point cloud data of three different workpiece surfaces collected by HDM are used for filtering analysis. Gaussian filter (ISO 11562:1996, ASME B46.1-2002), the FABEMD-based filter and the BEMD-based filter are applied respectively, and then the filtering performances of these three filters are analyzed.

The 3D Gaussian filter is a 3D extension of 2D Gaussian filter, which is realized by the convolution of 3D surface data and the 2D weight function. The weighting function of Gaussian filter for surface texture analysis is

$$S(x,y)=\frac{1}{\alpha^2\lambda_{xc}\lambda_{yc}}\exp[-\left[\pi(\frac{x}{\alpha\lambda_{xc}})^2+\pi(\frac{y}{\alpha\lambda_{yc}})^2\right]] \quad (19)$$

where $\lambda_{xc}$and λ_{yc} are the cutoff wavelengths in the x and y directions, and $\alpha=\sqrt{\ln 2/\pi}=0.4697$. In the paper, set $\lambda_{xc}=\lambda=0.64$mm.

In order to evaluate the characteristics of 3D surface topography, some representative 3D surface parameters are selected, including surface amplitude parameters S_a, S_q and S_t, surface shape parameters S_{ku}, and surface spacing parameters S_{al} and S_{tr}.

(1) Surface amplitude parameters

Surface amplitude parameter is the description of surface height deviations. The parameters S_a, S_q and S_t are selected.

The average roughness parameter S_a reflects the deviation of arithmetic mean distribution of the mean surface data

$$S_a=\frac{1}{A}\int\int_A |z(x,y)|dxdy \quad (20)$$

where $Z(x, y)$ is the height value of the point located in line x and column y and A is the evaluation area.

The root mean square roughness S_q is the standard deviation of the sample to reflect the surface roughness

$$S_q=\sqrt{\frac{1}{A}\int\int_A z^2(x,y)dxdy} \quad (21)$$

The maximum height of texture surface represents the maximum fluctuation of the sample surface

$$S_t=|\max(z(x,y))|+|\min(z(x,y))| \quad (22)$$

(2) Surface shape parameters

Surface shape parameters reflect the height shape characteristics of surface texture. Surface kurtosis S_{ku}reflects the surface height distribution

$$S_{ku}=\frac{1}{sq^4}[\frac{1}{A}\int\int_A z^2(x,y)dxdy] \quad (23)$$

(3) Surface spacing parameters

Surface spacing parameters reflect the spatial distribution of a sample surface. The fastest autocorrelation decay length S_{al} represents the composition of surface components, and $S_{al}\in(0,1)$. The smaller the value of S_{al} is, the bigger the probability of the surface with low frequency components is. The larger the value of S_{al} is, the bigger the probability of the surface with high frequency components is. S_{al} is the horizontal distance of the autocorrelation function (ACF) that has the fastest decay in any direction to a specified threshold value η, and $0<\eta<1$ ($\eta=0.1$ in this study).

$$S_{al}=\mathop{Min}_{\tau_x,\tau_y\in R}(\sqrt{\tau_x^2+\tau_y^2})\, where\, R=\{(\tau_x,\tau_y):ACF(\tau_x,\tau_y)\le\eta \quad (24)$$

The ACF of a 3D surface is defined as a convolution of the surface with itself

$$ACF(\tau_x,\tau_y)=\frac{\int\int_A z(x,y)z(x-\tau_x,y-\tau_y)dxdy}{\int\int_A z(x,y)z(x,y)dxdy} \quad (25)$$

where τ_x, τ_y are the x-direction and y-direction shifts respectively.

The surface texture aspect ratio parameter S_{tr} (Eq. (26)) reflects the surface texture characteristics of sample surface. The smaller the value of S_{tr} is, the more obvious the surface texture is. The larger the value of S_{tr} is, the less obvious the surface texture is.

$$S_{tr}=\frac{\mathop{Min}_{\tau_x,\tau_y\in R}(\sqrt{\tau_x^2+\tau_y^2})}{\mathop{Max}_{\tau_x,\tau_y\in R}(\sqrt{\tau_x^2+\tau_y^2})}\, where\, R=\{(\tau_x,\tau_y):ACF(\tau_{x,\tau_y})\le\eta \quad (26)$$

5.1. Case study I

The first workpiece surface is the surface of a pump valve plate, and its height map is shown in Fig. 9. A surface sample is arbitrarily selected from the surface, the size of the surface sample is 6.4 mm × 6.4 mm (shown in Fig. 10(a)) and the sampling interval is 0.01 mm. The results of the FABEMD-based filter are shown in Fig. 10. Fig. 10(b)–(d) represent roughness, waviness and form respectively.

Because of the boundary effects caused by the local weighted average in the Gaussian filter, the evaluation area of the Gaussian filter needs to be subtracted the first and last wavelengths from the sum in order to obtain good filtering results, and then the actual area becomes 5.12 mm × 5.12 mm. The surface sample is separated into two components: one component is the mean surface including the waviness surface and the form surface, and the other one is the roughness surface.

Fig. 11 presents a comparison of mean surfaces obtained by Gaussian filter and FABEMD-based filter without discarding any boundary region, and the actual size of evaluation area is 6.4 mm × 6.4 mm. Fig. 11(a) illustrates that the values on the boundary of the mean surface by Gaussian filter are close to zero

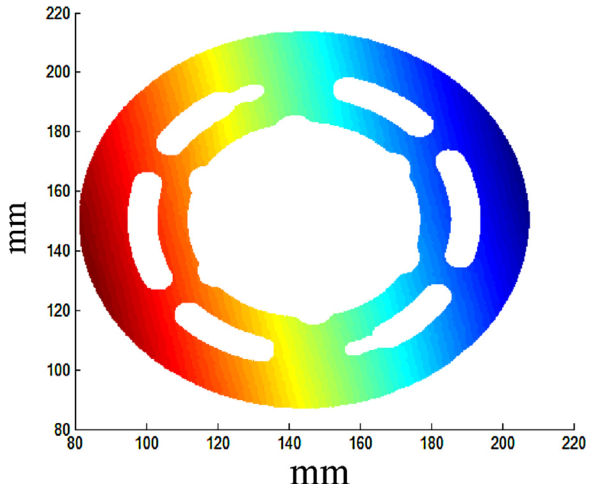

Fig. 9. The height map of the valve plate surface.

and there are obvious distortions on the boundary. This is the result of the convolution operation. As shown in Fig. 11(b), there is no distortion in the FABEMD filtering results. Therefore, due to the boundary effect of Gaussian filter, it is necessary to remove the boundary in practical application. It is feasible for the original data to be long enough. However, when the original data length is limited, and then the boundary area is given up, there will be inevitably some influences on the evaluation results. The FABEMD approach does not need to predict the extrema points on the boundary, so the boundary distortions are avoided. The FABEMD-based filter is more applicable than Gaussian filter.

Fig. 12 shows six samples of the oil pump valve, and the size of each sample surface is 6.4 mm × 6.4 mm. Then Gaussian filter, the FABEMD-based filter and the BEMD-based filter are applied to the six samples, and the filtering results are compared. To be convenient for the comparison, the actual evaluation area of three filters is set as 5.12 mm × 5.12 mm and the sampling interval is 0.01 mm.

Table 1 shows the surface amplitude parameters obtained by Gaussian filter and FABEMD-based filter. It can be found from the last three columns in Table 1 that the mean differences are close to 5% in S_a values, close to 4% in S_q values and close to 10% in $S_t$values.

Table 2 shows the surface amplitude parameters obtained by Gaussian filter and the BEMD-based filter. It can be found from the last three columns in Table 2 that the mean differences are close to 200% in S_a values, close to 190% in S_q values and close to 130% in S_t values. It can be seen that the mean differences of the surface amplitude parameters obtained by Gaussian filter and the FABEMD-based filter are less than 10%. Nevertheless, the mean differences of

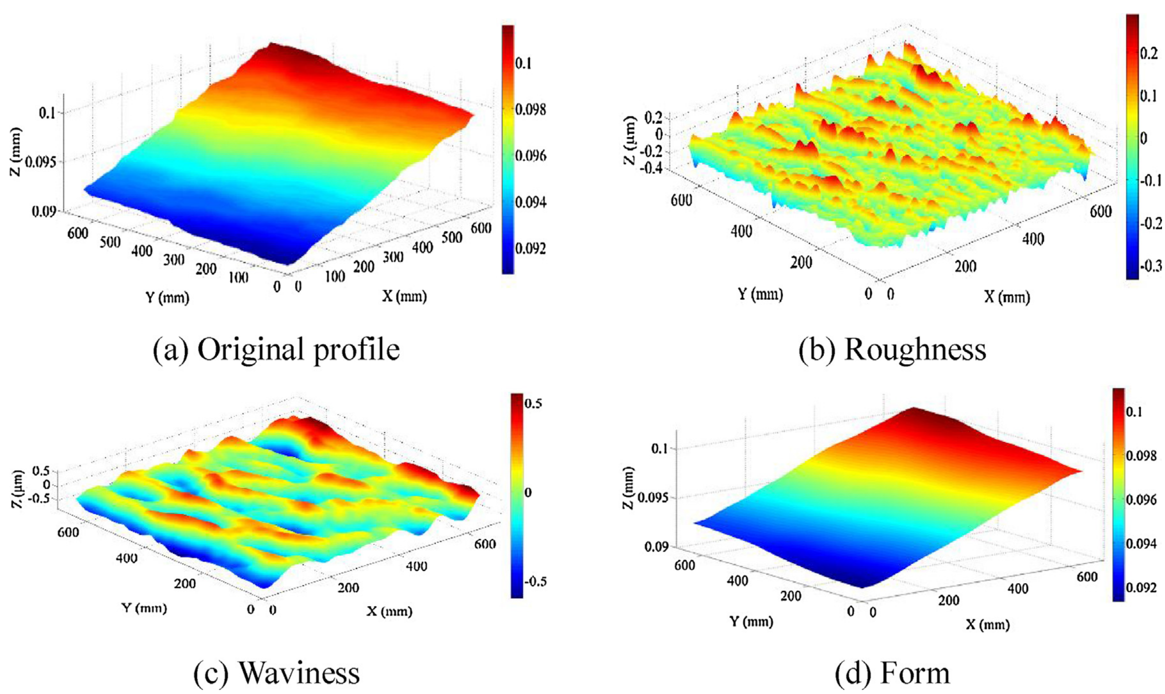

Fig. 10. Filtering results of a surface sample using the FABEMD filter.

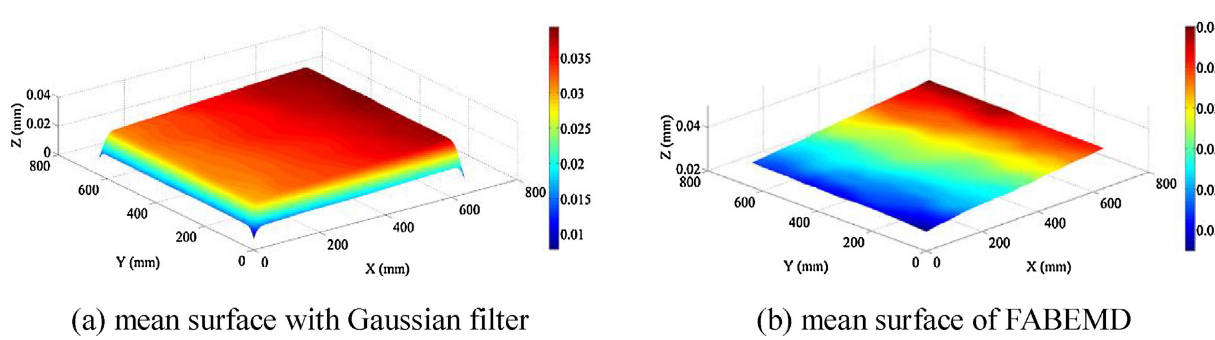

Fig. 11. Comparison of mean surfaces obtained by Gaussian filter and FABEMD.

Table 1
The comparison of surface amplitude parameters using the FABEMD-based filter and Gaussian filter.

Unit (um)	Gaussian filter			FABEMD-based filter			Difference		
	S_a	S_q	S_t	S_a	S_q	S_t	S_a	S_q	S_t
L_1	0.0405	0.0522	0.4367	0.0387	0.0507	0.4866	4.460%	2.779%	11.437%
L_2	0.0488	0.0643	0.6279	0.0468	0.0619	0.6239	4.090%	3.651%	0.632%
L_3	0.0413	0.0527	0.4678	0.0364	0.0478	0.5888	11.965%	9.315%	25.848%
L_4	0.0412	0.0532	0.5390	0.0397	0.0522	0.5570	3.600%	1.955%	3.340%
L_5	0.0422	0.0549	0.4816	0.0415	0.0542	0.5611	1.594%	1.224%	16.506%
L_6	0.0427	0.0556	0.6329	0.0411	0.0548	0.6145	3.809%	1.371%	2.900%
mean	0.0428	0.0555	0.5310	0.0407	0.0536	0.5720	4.920%	3.382%	10.111%

Difference is calculated by: $\left|\frac{\text{NFABEMDvalue}-\text{Gaussian value}}{\text{Gaussian value}}\right| \times 100\%$.

Table 2
The comparison of surface amplitude parameters using original BEMD-based filter and Gaussian filter.

Unit (um)	Gaussian filter			Original BEMD filter			Difference		
	S_a	S_q	S_t	S_a	S_q	S_t	S_a	S_q	S_t
L_1	0.0405	0.0522	0.4367	0.1276	0.1632	1.1715	215.208%	212.657%	168.277%
L_2	0.0488	0.0643	0.6279	0.1453	0.1811	1.1899	197.975%	181.751%	89.513%
L_3	0.0413	0.0527	0.4678	0.1235	0.1558	1.1604	199.075%	195.436%	148.022%
L_4	0.0412	0.0532	0.5390	0.1304	0.1653	1.2846	216.821%	210.692%	138.344%
L_5	0.0422	0.0549	0.4816	0.1215	0.1535	1.0845	187.952%	179.418%	125.184%
L_6	0.0427	0.0556	0.6329	0.1250	0.1573	1.2452	192.632%	182.914%	96.762%
mean	0.0428	0.0555	0.5310	0.1289	0.1627	1.1894	201.610%	193.811%	127.684%

Table 3
The comparison of surface shape and surface space parameters using the FABEMD-based filter and Gaussian filter.

	Gaussian filter			FABEMD-based filter			Difference		
	S_{ku}	S_{al}	S_{tr}	S_{ku}	S_{al}	S_{tr}	S_{ku}	S_{al}	S_{tr}
L_1	3.4910	10.7703	0.5038	3.9946	9.4868	0.4543	14.424%	11.917%	9.821%
L_2	4.2383	10.1980	0.4079	4.3547	9.4340	0.3594	2.746%	7.492%	11.893%
L_3	3.5110	10.1980	0.5036	4.4378	8.5440	0.4220	26.399%	16.219%	16.219%
L_4	3.8398	10.0499	0.3766	4.3204	8.9443	0.3720	12.516%	11.001%	1.222%
L_5	3.8443	10.1980	0.4122	3.9735	8.9443	0.3874	3.360%	12.294%	6.019%
L_6	4.2349	10.0499	0.5575	4.4616	8.9443	0.4339	5.353%	11.001%	22.173%
mean	3.8599	10.2440	0.4603	4.2571	9.0496	0.4048	10.800%	11.654%	11.224%

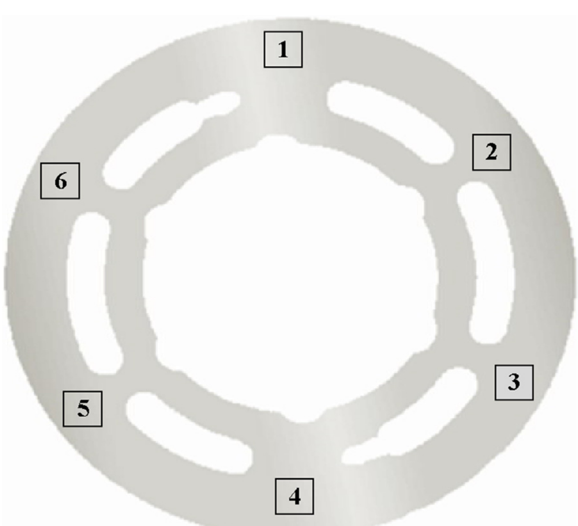

Fig. 12. The distribution map of six sample surface.

the surface amplitude parameters obtained by Gaussian filter and the original BEMD-based filter are about 130%–200%. Therefore, the FABEMD-based filter can reflect the sample surface amplitude, but the BEMD-based filter cannot reflect the sample surface amplitude.

Table 3 shows the surface shape and spacing parameters obtained by Gaussian filter and the FABEMD-based filter. It can be found from the last three columns in Table 3 that the mean differences are close to 11% in S_{ku} values, close to 12% in S_{al} values and close to 11% in S_{tr}values. In general, the mean differences of shape parameters and spacing parameters are within 20%.

Table 4 shows the surface shape and spacing parameters obtained by Gaussian filter and the FABEMD-based filter. It can be found from the last three columns in Table 4 that the mean differences are close to 18% in S_{ku} values, close to 100% in S_{al} values and close to 15% in S_{tr}values.

Table 5 lists the comparison results of the window width and computational time using the BEMD-based filter and FABEMD-based filter. It can be found that the optimal window width of the order statistics filters searched by the FABEMD-based filter is 15 or 17. That is to say, the window width of the order statistics filter is relatively stable in the filtering process, which means that the surface topography of the workpieces is more uniform. However, the window width of the order statistics filters searched by the BEMD-based ranges from 57 to 69 and the filter window width changes greatly, which cannot reflect the surface topography. Moreover, the filtering time of the FABEMD-based filter is less than 30% of the filtering time of the BEMD-based filter, so the computational efficiency is improved.

5.2. Case study II

The second surface is the joint surface of an engine cylinder head, which is made of aluminum. The height map of this surface is shown in Fig. 13. Eight locations are selected (shown in Fig. 14)

Table 4
The comparison of surface shape and surface space parameters using the BEMD-based filter and Gaussian filter.

	Gaussian filter			BEMD-based filter			Difference		
	S_{ku}	S_{al}	S_{tr}	S_{ku}	S_{al}	S_{tr}	S_{ku}	S_{al}	S_{tr}
L_1	3.4910	10.7703	0.5038	3.3864	21.1896	0.4156	2.998%	96.741%	17.517%
L_2	4.2383	10.1980	0.4079	2.8532	18.9737	0.3518	32.680%	86.052%	13.761%
L_3	3.5110	10.1980	0.5036	3.1626	19.6469	0.4154	9.923%	92.654%	17.522%
L_4	3.8398	10.0499	0.3766	3.3659	21.8403	0.3608	12.342%	117.319%	4.201%
L_5	3.8443	10.1980	0.4122	3.0063	19.1050	0.3835	21.799%	87.340%	6.974%
L_6	4.2349	10.0499	0.5575	3.0917	20.2485	0.4129	26.996%	101.480%	25.935%
Mean	3.8599	10.2440	0.4603	3.1443	20.1673	0.3900	17.790%	96.931%	14.318%

Table 5
The comparison of window width and computational time using the BEMD-based filter and FABEMD-based filter.

Comparative item	Gaussian filter	BEMD-based filter		FABEMD-based filter		Time scale
	Time/s	Original window size	Time/s	Optimal window size	Time/s	
L_1	88	59	412	17	94	22.82%
L_2	145	57	407	17	172	42.26%
L_3	93	63	407	15	96	23.59%
L_4	90	69	546	15	90	16.48%
L_5	87	59	326	17	99	30.37%
L_6	89	61	437	17	95	21.74%
mean	98.67	–	422.5	–	107.67	26.20%

Time scale is calculated by: $\left|\frac{\text{NFABEMD Time} - \text{BEMDTime}}{\text{BEMDTime}}\right| \times 100\%$.

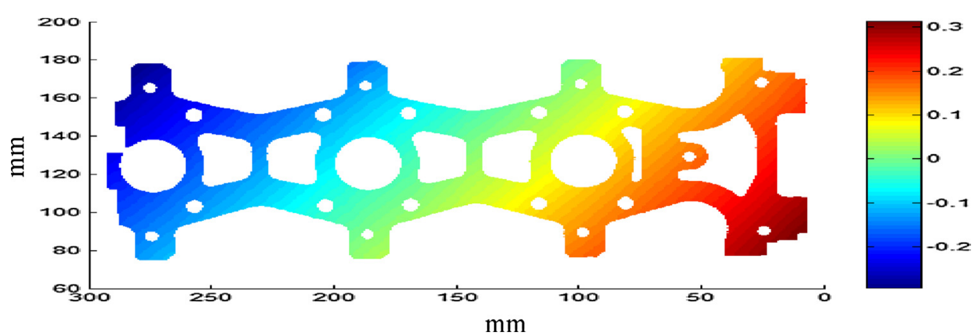

Fig. 13. The height map of the engine cylinder head.

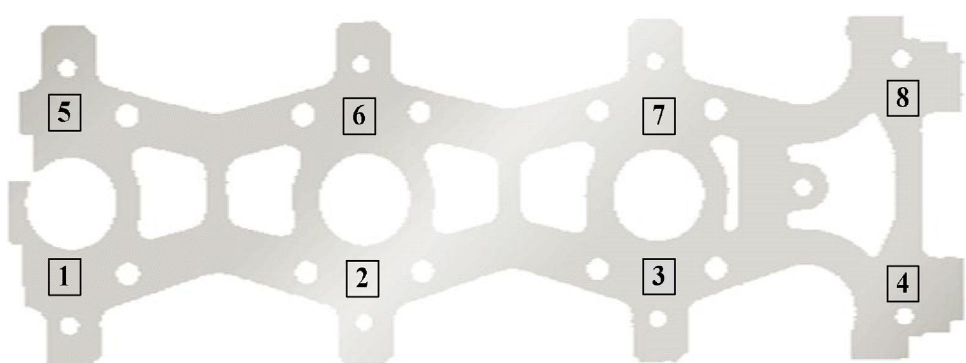

Fig. 14. The distribution map of eight sample surfaces.

from this surface with the same size and then eight small surfaces are obtained. Then Gaussian filter, the FABEMD-based filter and BEMD-based filter are applied to the eight sample surfaces and the surface texture parameters are obtained by the three filters.

Table 6 shows the surface amplitude parameters obtained by Gaussian filter and the FABEMD-based filter. It can be found from the last three columns in Table 6 that the mean differences are close to 4% in S_a values, close to 5% in S_q values and close to 13% in $S_t$values. Table 7 shows the surface amplitude parameters obtained by Gaussian filter and the BEMD-based filter. It can be found from the last three columns in Table 7 that the mean differences are close to 320% in S_a values, close to 320% in S_q values and close to 250% in $S_t$values.

Table 8 shows the surface shape and spacing parameters obtained by Gaussian filter and the FABEMD-based filter. It can be found from the last three columns in Table 8 that the mean differences are close to 17% in S_{ku} values, close to 15% in S_{al} values and close to 18% in S_{tr} values. In general, the mean differences of shape parameters and spacing parameters are within 20% [7,8].

Table 6
The comparison of surface amplitude parameters using the FABEMD-based filter and Gaussian filter.

Unit (um)	Gaussian filter			FABEMD-based filter			Difference		
	S_a	S_q	S_t	S_a	S_q	S_t	S_a	S_q	S_t
L_1	0.0534	0.0690	0.6682	0.0539	0.0707	0.7618	0.976%	2.507%	14.008%
L_2	0.0539	0.0685	0.5922	0.0565	0.0731	0.636	4.838%	6.595%	7.396%
L_3	0.0558	0.0728	0.7431	0.0583	0.0785	0.8556	4.482%	7.783%	15.139%
L_4	0.0589	0.0752	0.5977	0.0591	0.0764	0.655	0.266%	1.650%	9.587%
L_5	0.0540	0.0698	0.6117	0.0516	0.0681	0.7514	4.344%	2.469%	22.838%
L_6	0.0651	0.0863	0.8597	0.0617	0.0846	0.9325	5.253%	1.976%	8.468%
L_7	0.0605	0.0796	0.8109	0.0640	0.0869	0.9489	5.717%	9.196%	17.018%
L_8	0.0682	0.0880	0.7744	0.0724	0.0949	0.854	6.253%	7.950%	10.279%
mean	0.0587	0.0761	0.7072	0.0597	0.0792	0.7994	4.016%	5.016%	13.092%

Table 7
The comparison of surface amplitude parameters using the BEMD-based filter and Gaussian filter.

Unit (um)	Gaussian filter			BEMD-based filter			Difference		
	S_a	S_q	S_t	S_a	S_q	S_t	S_a	S_q	S_t
L_1	0.0534	0.0690	0.6682	0.2002	0.2601	2.0383	274.797%	276.852%	205.047%
L_2	0.0539	0.0685	0.5922	0.2136	0.2861	2.2826	295.948%	317.471%	285.447%
L_3	0.0558	0.0728	0.7431	0.2466	0.3125	2.4807	341.940%	329.037%	233.842%
L_4	0.0589	0.0752	0.5977	0.2733	0.3446	2.3799	363.976%	358.349%	298.162%
L_5	0.0540	0.0698	0.6117	0.2565	0.3266	2.8264	375.294%	367.791%	362.017%
L_6	0.0651	0.0863	0.8597	0.2912	0.3512	2.2874	347.392%	307.100%	166.080%
L_7	0.0605	0.0796	0.8109	0.2234	0.2915	2.2083	269.052%	266.361%	172.310%
L_8	0.0682	0.0880	0.7744	0.2888	0.3607	2.6552	323.665%	310.142%	242.867%
mean	0.0587	0.0761	0.7072	0.2492	0.3167	2.3948	324.008%	316.638%	245.721%

Table 8
The comparison of surface space parameters using FABEMD filter and Gaussian filter.

	Gaussian filter			FABEMD-based filter			Difference		
	S_{ku}	S_{al}	S_{tr}	S_{ku}	S_{al}	S_{tr}	S_{ku}	S_{al}	S_{tr}
L_1	3.7896	10.2956	0.3463	4.2491	8.4853	0.2666	12.125%	17.584%	23.010%
L_2	3.2838	9.4340	0.2964	3.8343	8.4853	0.2606	16.763%	10.056%	12.073%
L_3	3.9827	9.8995	0.3255	5.1213	8.4853	0.2666	28.588%	14.286%	18.093%
L_4	3.3280	9.8995	0.3041	3.6743	8.4853	0.2553	10.404%	14.286%	16.049%
L_5	3.6304	10.6301	0.3067	4.1058	8.4853	0.2352	13.094%	20.177%	23.306%
L_6	4.2649	9.8995	0.2791	5.0170	8.4853	0.2306	17.633%	14.286%	17.380%
L_7	4.1878	10.0000	0.2881	5.4650	8.4853	0.2599	30.497%	15.147%	9.784%
L_8	3.6529	10.6301	0.3220	3.8548	9.8489	0.2616	5.528%	7.350%	18.740%
mean	3.7650	10.0860	0.3085	4.4152	8.6557	0.2546	16.829%	14.146%	17.305%

Table 9
The comparison of surface space parameters using the BEMD-based filter and Gaussian filter.

	Gaussian filter			BEMD-based filter			Difference		
	S_{ku}	S_{al}	S_{tr}	S_{ku}	S_{al}	S_{tr}	S_{ku}	S_{al}	S_{tr}
L_1	3.7896	10.2956	0.3463	3.6244	25.0000	0.4595	4.359%	142.821%	32.699%
L_2	3.2838	9.4340	0.2964	4.3492	28.2843	0.4650	32.445%	199.813%	56.875%
L_3	3.9827	9.8995	0.3255	3.6657	27.2029	0.4415	7.960%	174.791%	35.629%
L_4	3.3280	9.8995	0.3041	2.9795	30.4795	0.4771	10.473%	207.889%	56.896%
L_5	3.6304	10.6301	0.3067	3.5005	29.1548	0.3586	3.578%	174.265%	16.907%
L_6	4.2649	9.8995	0.2791	2.3775	29.6985	0.3420	44.254%	200.000%	22.531%
L_7	4.1878	10.0000	0.2881	3.6887	21.6333	0.3529	11.919%	116.333%	22.517%
L_8	3.6529	10.6301	0.3220	3.0149	30.4138	0.3679	17.466%	186.109%	14.272%
mean	3.7650	10.0860	0.3085	3.4000	27.7334	0.4081	16.557%	175.253%	32.291%

Table 9 shows the surface shape and spacing parameters obtained by Gaussian filter and the FABEMD-based filter. It can be found from the last three columns in Table 9 that the mean differences are close to 17% in S_{ku}values, close to 175% in S_{al} values and close to 32% in S_{tr} values.

Table 10 shows the comparison results of the window width and computational time using the BEMD-based filter and FABEMD-based filter. It can be seen that the optimal window width of the order statistics filters searched by the FABEMD-based filter is 15 or 17. That is to say, the window width of the order statistics filter is relatively stable in the filtering process, which means that the surface topography of the workpieces is more uniform. The window width of the order statistics filters searched by the BEMD-based filter ranges from 63 to 99 and the filter window width changes greatly, which cannot reflect the surface topography of the workpieces. Moreover, the filtering time of the FABEMD-based filter is less than 15% of the BEMD-based filter's filtering time, so the computational efficiency is improved.

Table 10
The comparison of window width and computational time using the BEMD-based filter and FABEMD-based filter.

Comparative item	Gaussian filter	BEMD-based filter		FABEMD-based filter		Time scale
	Time/s	Original window size	Time/s	Optimal window size	Time/s	
L_1	115	77	602	15	130	21.59%
L_2	79	83	677	15	82	12.11%
L_3	129	81	1521	15	134	8.81%
L_4	247	99	1546	15	267	17.27%
L_5	88	89	864	15	88	10.19%
L_6	59	75	587	15	57	9.71%
L_7	79	63	400	15	101	25.25%
L_8	56	91	840	17	61	7.26%
mean	106.5	–	879.63	–	115	14.02%

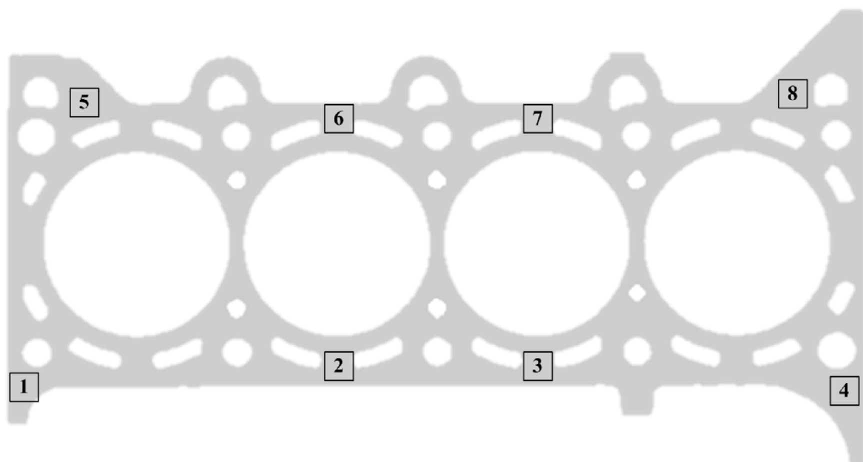

Fig. 15. The distribution map of eight sample surface.

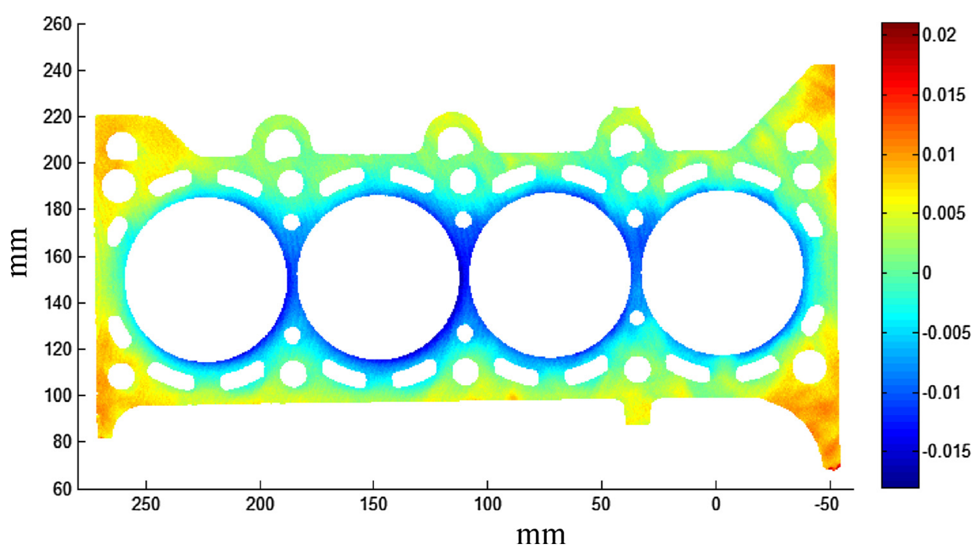

Fig. 16. The height map of the top surface of an engine cylinder block.

5.3. *Case study III*

The third surface is the top surface of an engine cylinder block, which is made of cast iron FC250. Eight locations (shown in Fig. 15) from three top surfaces of engine blocks A, B, and C using HDM (shown in Fig. 16) are selected. Then Gaussian filter, the FABEMD-based filter and BEMD-based filter are applied to the eight sample surfaces and the surface texture parameters are obtained by the three filters.

Table 11 shows the surface amplitude parameters obtained by Gaussian filter and the FABEMD-based filter. It can be found from the last three columns in Table 11 that the mean differences are close to 6% in S_a values, close to 6% in S_q values and close to 15% in $S_t$values. Table 12 shows the surface amplitude parameters obtained by Gaussian filter and the BEMD-based filter. It can be found from the last three columns in Table 12 that the mean differences are close to 80% in S_a values, close to 70% in S_q values and close to 20% in $S_t$values.

Table 11
The comparison of surface amplitude parameters using the FABEMD-based filter and Gaussian filter.

Unit (um)	Gaussian filter			FABEMD-based filter			Difference		
	S_a	S_q	S_t	S_a	S_q	S_t	S_a	S_q	S_t
A_1	0.1156	0.1651	2.6943	0.1116	0.1554	2.4564	3.459%	5.898%	8.828%
A_2	0.1183	0.1622	2.1284	0.1104	0.1563	1.9070	6.710%	3.620%	10.401%
A_3	0.1398	0.1887	2.0661	0.1315	0.1756	1.7277	5.955%	6.957%	16.380%
A_4	0.1399	0.1901	1.8789	0.1322	0.1819	2.1565	5.529%	4.310%	14.774%
A_5	0.1600	0.2139	2.4569	0.1513	0.2017	2.1235	5.440%	5.699%	13.569%
A_6	0.1119	0.1581	2.1261	0.1096	0.1544	2.4022	2.108%	2.296%	12.988%
A_7	0.1379	0.1848	1.9595	0.1321	0.1746	1.5903	4.233%	5.538%	18.843%
A_8	0.1428	0.1935	1.9830	0.1318	0.1772	1.7560	7.735%	8.422%	11.447%
mean	0.1333	0.1821	2.1616	0.1263	0.1721	2.0150	5.146%	5.343%	13.404%
B_1	0.1452	0.1994	2.0488	0.1361	0.1858	2.2308	6.262%	6.818%	8.883%
B_2	0.1361	0.1854	2.3379	0.1220	0.1679	2.2269	10.320%	9.461%	4.748%
B_3	0.1468	0.1960	1.7773	0.1392	0.1860	1.6384	5.163%	5.115%	7.816%
B_4	0.1557	0.2109	2.2060	0.1455	0.1970	2.0811	6.557%	6.572%	5.663%
B_5	0.1622	0.2219	2.7310	0.1513	0.2060	2.2255	6.761%	7.162%	18.509%
B_6	0.1447	0.1910	2.0815	0.1415	0.1877	1.7823	2.198%	1.749%	14.374%
B_7	0.1601	0.2105	2.0696	0.1507	0.1985	2.1003	5.897%	5.686%	1.484%
B_8	0.1563	0.2093	2.2703	0.1497	0.1975	1.8803	4.191%	5.596%	17.178%
mean	0.1509	0.2031	2.1903	0.1420	0.1908	2.0207	5.918%	6.020%	9.832%
C_1	0.1474	0.2101	2.9192	0.1390	0.1925	2.4003	5.738%	8.388%	17.776%
C_2	0.1266	0.1719	2.0016	0.1320	0.1765	1.7630	4.277%	2.661%	11.924%
C_3	0.1308	0.1794	2.2440	0.1267	0.1709	2.0207	3.153%	4.749%	9.950%
C_4	0.1370	0.1885	2.3623	0.1362	0.1902	2.8634	0.615%	0.925%	21.213%
C_5	0.1369	0.1872	2.2162	0.1389	0.1864	1.9199	1.441%	0.429%	13.370%
C_6	0.1211	0.1648	1.7526	0.1192	0.1605	1.6505	1.577%	2.596%	5.822%
C_7	0.1397	0.1883	2.1512	0.1419	0.1898	1.9103	1.522%	0.784%	11.198%
C_8	0.1476	0.2032	2.3495	0.1473	0.2023	2.1238	0.188%	0.419%	9.604%
mean	0.1359	0.1867	2.2496	0.1351	0.1836	2.0815	2.314%	2.619%	12.607%

Table 12
The comparison of surface amplitude parameters using the BEMD-based filter and Gaussian filter.

Unit (um)	Gaussian filter			BEMD-based filter			Difference		
	S_a	S_q	S_t	S_a	S_q	S_t	S_a	S_q	S_t
A_1	0.1156	0.1651	2.6943	0.1833	0.2410	3.0396	58.471%	45.918%	12.816%
A_2	0.1183	0.1622	2.1284	0.2337	0.3000	2.5406	97.484%	84.992%	19.369%
A_3	0.1398	0.1887	2.0661	0.2306	0.2873	2.2990	64.982%	52.206%	11.273%
A_4	0.1399	0.1901	1.8789	0.2288	0.2944	2.3113	63.567%	54.861%	23.011%
A_5	0.1600	0.2139	2.4569	0.2410	0.3034	2.4455	50.683%	41.843%	0.463%
A_6	0.1119	0.1581	2.1261	0.2089	0.2708	2.9939	86.706%	71.322%	40.821%
A_7	0.1379	0.1848	1.9595	0.2240	0.2786	2.0193	62.363%	50.697%	3.050%
A_8	0.1428	0.1935	1.9830	0.2379	0.2992	2.3661	66.599%	54.662%	19.320%
mean	0.1333	0.1821	2.1616	0.2235	0.2843	2.5019	68.857%	57.062%	16.265%
B_1	0.1452	0.1994	2.0488	0.2356	0.3034	2.6825	62.252%	52.123%	30.926%
B_2	0.1361	0.1854	2.3379	0.2404	0.3073	2.5096	76.705%	65.719%	7.342%
B_3	0.1468	0.1960	1.7773	0.2428	0.3052	2.1047	65.424%	55.710%	18.425%
B_4	0.1557	0.2109	2.2060	0.2516	0.3191	2.2775	61.613%	51.315%	3.243%
B_5	0.1622	0.2219	2.7310	0.2836	0.3584	2.7291	74.820%	61.539%	0.068%
B_6	0.1447	0.1910	2.0815	0.2413	0.3031	2.6128	66.786%	58.665%	25.527%
B_7	0.1601	0.2105	2.0696	0.2443	0.3056	2.4334	52.525%	45.148%	17.581%
B_8	0.1563	0.2093	2.2703	0.2435	0.3045	2.6625	55.805%	45.525%	17.274%
mean	0.1509	0.2031	2.1903	0.2479	0.3133	2.5015	64.491%	54.468%	15.048%
C_1	0.1474	0.2101	2.9192	0.2371	0.3012	2.7601	60.801%	43.347%	5.452%
C_2	0.1266	0.1719	2.0016	0.2377	0.2972	2.0208	87.728%	72.879%	0.955%
C_3	0.1308	0.1794	2.2440	0.2027	0.2565	2.1661	54.949%	42.966%	3.471%
C_4	0.1370	0.1885	2.3623	0.2533	0.3296	3.5874	84.893%	74.879%	51.859%
C_5	0.1369	0.1872	2.2162	0.2471	0.3083	2.3451	80.539%	64.743%	5.816%
C_6	0.1211	0.1648	1.7526	0.2093	0.2595	1.9339	72.831%	57.537%	10.347%
C_7	0.1397	0.1883	2.1512	0.2631	0.3264	2.1417	88.277%	73.282%	0.439%
C_8	0.1476	0.2032	2.3495	0.2584	0.3273	2.5157	75.072%	61.081%	7.074%
mean	0.1359	0.1867	2.2496	0.2386	0.3008	2.4338	75.636%	61.339%	10.677%

Table 13 shows the surface shape and spacing parameters obtained by Gaussian filter and the FABEMD filter. It can be found from the last three columns in Table 13 that the mean differences are close to 15% in S_{ku} values, close to 10% in S_{al} values and close to 10% in S_{tr} values. Table 14 shows the surface shape and spacing parameters obtained by Gaussian filter and the FABEMD-based filter. It can be found from the last three columns in Table 14 that the mean differences are close to 40% in S_{ku} values, close to 60% in S_{al} values and close to 20% in S_{tr} values.

Table 15 shows the comparison results of the window width and computational time using the BEMD-based filter and FABEMD-based filter. It can be seen that the optimal window width of the order statistics filters searched by the FABEMD filter is 17 or 19. That is to say, the window width of the order statistics filter is relatively stable in the filtering process, which means that the surface topography of the workpieces is more uniform. However, the window width of the order statistics filters searched by the BEMD-based filter ranges from 41 to 53 and the filter window width changes

Table 13
The comparison of surface shape and surface space parameters using the FABEMD-based filter and Gaussian filter.

	Gaussian filter			FABEMD-based filter			Difference		
	S_{ku}	S_{al}	S_{tr}	S_{ku}	S_{al}	S_{tr}	S_{ku}	S_{al}	S_{tr}
A_1	9.1148	9.8995	0.8682	6.7925	9.8489	0.8705	25.478%	0.512%	0.263%
A_2	5.0939	10.2956	0.8435	5.6636	9.2195	0.7199	11.185%	10.452%	14.645%
A_3	4.5250	8.9443	0.6293	4.0407	8.4853	0.5970	10.703%	5.132%	5.132%
A_4	4.5382	10.1980	0.9014	4.7112	9.8489	0.9105	3.811%	3.424%	1.014%
A_5	4.5811	8.9443	0.6984	4.1437	8.6023	0.6717	9.549%	3.823%	3.823%
A_6	5.6777	9.4340	0.9434	5.7261	8.9443	0.9701	0.853%	5.191%	2.835%
A_7	4.3867	9.2195	0.7656	3.8753	9.2195	0.8086	11.657%	0.000%	5.612%
A_8	4.4407	8.6023	0.6083	4.1878	7.8102	0.5254	5.695%	9.208%	13.629%
mean	5.2948	9.4422	0.7823	4.8926	8.9974	0.7592	9.867%	4.718%	5.869%
B_1	4.7258	9.8489	0.8179	4.7322	9.8489	0.8638	0.136%	0.000%	5.612%
B_2	5.3655	9.8489	0.9105	5.2404	9.2195	0.8673	2.331%	6.390%	4.747%
B_3	4.2510	9.2195	0.6487	4.0750	8.4853	0.5970	4.140%	7.964%	7.964%
B_4	4.4152	10.4403	0.9338	4.5338	10.0499	0.9454	2.686%	3.740%	1.243%
B_5	5.0360	9.2195	0.6778	4.3764	9.2195	0.7199	13.098%	0.000%	6.210%
B_6	3.9728	10.0499	0.9761	3.8823	9.8489	0.9849	2.278%	2.000%	0.897%
B_7	3.9866	9.4340	0.8274	3.9565	9.4340	0.8274	0.755%	0.000%	0.000%
B_8	4.5384	8.9443	0.6576	3.9084	8.4853	0.6307	13.881%	5.132%	4.089%
mean	4.5364	9.6257	0.8062	4.3381	9.3239	0.8046	4.913%	3.153%	3.845%
C_1	7.3363	9.8489	0.8638	5.3702	9.8489	0.9105	26.800%	0.000%	5.409%
C_2	5.0942	9.8489	0.8638	4.2327	9.8489	0.8179	16.911%	0.000%	5.314%
C_3	5.2124	8.4853	0.5970	4.4603	8.4853	0.5708	14.430%	0.000%	4.395%
C_4	5.3706	10.0499	0.8883	6.0444	10.0499	0.9454	12.545%	0.000%	6.430%
C_5	5.0714	9.2195	0.6853	4.2062	8.9443	0.6648	17.061%	2.986%	2.986%
C_6	4.7760	9.8489	0.9849	4.2548	9.8489	0.9849	10.913%	0.000%	0.000%
C_7	4.4940	9.4340	0.7834	4.0786	9.8489	0.8638	9.243%	4.398%	10.256%
C_8	5.0301	8.4853	0.5708	4.4833	8.4853	0.5708	10.871%	0.000%	0.000%
mean	5.2981	9.4026	0.7797	4.6413	9.4200	0.7911	14.847%	0.923%	4.349%

Table 14
The comparison of surface shape and surface space parameters using BEMD filter and Gaussian filter.

	Gaussian filter			BEMD-based filter			Difference		
	S_{ku}	S_{al}	S_{tr}	S_{ku}	S_{al}	S_{tr}	S_{ku}	S_{al}	S_{tr}
A_1	9.1148	9.8995	0.8682	4.6746	13.8924	0.8786	48.715%	40.335%	1.197%
A_2	5.0939	10.2956	0.8435	3.5070	15.0000	0.4779	31.152%	45.693%	43.335%
A_3	4.5250	8.9443	0.6293	2.9224	13.4164	0.6448	35.416%	50.000%	2.453%
A_4	4.5382	10.1980	0.9014	3.3547	14.0357	0.8158	26.079%	37.631%	9.494%
A_5	4.5811	8.9443	0.6984	3.0721	12.5300	0.7640	32.940%	40.089%	9.383%
A_6	5.6777	9.4340	0.9434	4.0292	15.2971	0.7351	29.035%	62.148%	22.076%
A_7	4.3867	9.2195	0.7656	2.8634	14.1421	0.8771	34.725%	53.393%	14.552%
A_8	4.4407	8.6023	0.6083	3.0115	12.2066	0.6028	32.183%	41.898%	0.894%
mean	5.2948	9.4422	0.7823	3.4294	13.8150	0.7245	33.781%	46.398%	12.923%
B_1	4.7258	9.8489	0.8179	3.3730	13.9284	0.7726	28.627%	41.421%	5.538%
B_2	5.3655	9.8489	0.9105	3.1891	15.5242	0.8082	40.562%	57.624%	11.243%
B_3	4.2510	9.2195	0.6487	2.9632	13.0000	0.6055	30.294%	41.005%	6.662%
B_4	4.4152	10.4403	0.9338	3.1491	13.9284	0.7726	28.676%	33.410%	17.263%
B_5	5.0360	9.2195	0.6778	3.0794	15.0333	0.7622	38.853%	63.059%	12.449%
B_6	3.9728	10.0499	0.9761	3.0651	14.3178	0.6501	22.848%	42.468%	33.396%
B_7	3.9866	9.4340	0.8274	2.9785	13.6015	0.9212	25.288%	44.175%	11.336%
B_8	4.5384	8.9443	0.6576	2.9789	12.2066	0.7334	34.363%	36.473%	11.531%
mean	4.5364	9.6257	0.8062	3.0970	13.9425	0.7532	31.189%	44.954%	13.677%
C_1	7.3363	9.8489	0.8638	3.4618	14.1421	0.8623	52.813%	43.592%	0.178%
C_2	5.0942	9.8489	0.8638	2.8783	15.2315	0.6325	43.499%	54.653%	26.782%
C_3	5.2124	8.4853	0.5970	3.1265	12.0416	0.6303	40.019%	41.912%	5.572%
C_4	5.3706	10.0499	0.8883	3.8724	15.8114	0.8380	27.896%	57.329%	5.661%
C_5	5.0714	9.2195	0.6853	2.9632	14.5602	0.7828	41.570%	57.928%	14.225%
C_6	4.7760	9.8489	0.9849	2.8417	15.1327	0.7921	40.501%	53.650%	19.576%
C_7	4.4940	9.4340	0.7834	2.7657	16.0312	0.7491	38.456%	69.931%	4.386%
C_8	5.0301	8.4853	0.5708	3.0339	13.4164	0.6202	39.685%	58.114%	8.653%
mean	5.2981	9.4026	0.7797	3.1179	14.5459	0.7384	40.555%	54.638%	10.629%

greatly, which cannot reflect the surface topography of the parts. Moreover, the filtering time of FABEMD filter is less than 50% of the BEMD filter's filtering time, so the computational efficiency is improved.

It can be seen from the above three cases that the differences of the surface texture parameters between Gaussian filter and the BEMD-based filter are relatively large. So the BEMD-based filter cannot be directly applied to workpiece surface separations. Nevertheless, for Gaussian filter and the FABEMD-based filter, their differences of the average roughness parameter S_a and the root mean square roughness parameter S_q are close to 6%, and the maximum height of texture surface S_t is less than 20%. Moreover, the surface shape parameters S_{ku} and the surface spacing parameters S_{al} and S_t are also less than 20%. Because the difference of 10–20% is very common as reported in [7,8], so the results of three real-world surface data show that the performance of the FABEMD-based filter is similar to the performance of the standard Gaussian filer, but

Table 15
The comparison of window width and computational time using the BEMD-based filter and FABEMD-based filter.

Comparative item	Gaussian filter	BEMD-based filter		FABEMD-based filter		Time scale
	Time/s	Original window size	Time/s	Optimal window size	Time/s	
A_1	132	47	292	19	149	51.03%
A_2	136	47	278	17	140	50.36%
A_3	213	49	622	19	220	35.37%
A_4	176	45	268	19	204	76.12%
A_5	179	43	249	19	185	74.30%
A_6	197	47	484	17	220	45.45%
A_7	248	47	293	19	294	100.34%
A_8	101	47	361	17	109	30.19%
mean	172.75	–	355.88	–	190.13	57.90%
B_1	144	51	460	19	154	33.48%
B_2	145	51	393	17	150	38.17%
B_3	157	53	479	19	170	35.49%
B_4	138	47	312	19	151	48.40%
B_5	196	55	385	19	200	51.95%
B_6	143	47	330	19	162	49.09%
B_7	123	41	260	19	140	53.85%
B_8	157	47	285	19	174	61.05%
mean	150.375	–	363	–	162.63	46.43%
C_1	233	45	437	19	258	59.04%
C_2	212	47	587	19	240	40.89%
C_3	199	41	442	19	210	47.51%
C_4	317	51	525	19	321	61.14%
C_5	123	51	407	19	152	37.35%
C_6	137	47	312	19	142	45.51%
C_7	159	51	366	19	172	46.99%
C_8	163	51	367	19	189	51.50%
mean	192.86	–	430.38	–	210.5	48.74%

Table 16
The comparison of surface amplitude parameters using shearlet-based filter and Gaussian filter.

Unit (um)	Shearlet filter			Gaussian filter			Difference		
	S_a	S_q	S_t	S_a	S_q	S_t	S_a	S_q	S_t
L_1	0.036	0.047	0.524	0.041	0.052	0.437	12.099%	9.770%	19.876%
L_2	0.043	0.058	0.663	0.049	0.064	0.628	12.500%	9.798%	5.654%
L_3	0.037	0.049	0.512	0.041	0.053	0.468	10.412%	7.590%	9.470%
L_4	0.037	0.049	0.525	0.041	0.053	0.539	11.165%	8.835%	2.579%
L_5	0.038	0.051	0.499	0.042	0.055	0.482	9.953%	8.015%	3.571%
L_6	0.039	0.052	0.778	0.043	0.056	0.633	9.602%	6.115%	22.926%
mean	0.038	0.051	0.583	0.043	0.055	0.531	10.955%	8.354%	10.679%

Table 17
The comparison of surface shape and surface space parameters using shearlet-based filter and Gaussian filter.

	Shearlet filter			Gaussian filter			Difference		
	S_{ku}	S_{al}	S_{tr}	S_{ku}	S_{al}	S_{tr}	S_{ku}	S_{al}	S_{tr}
L_1	4.333	8.944	0.640	3.491	10.770	0.504	24.128%	16.954%	27.114%
L_2	5.095	8.544	0.540	4.238	10.198	0.408	20.211%	16.219%	32.483%
L_3	4.289	8.246	0.592	3.511	10.198	0.504	22.156%	19.139%	17.554%
L_4	4.337	8.246	0.478	3.840	10.050	0.377	12.951%	17.947%	26.845%
L_5	4.464	8.246	0.566	3.844	10.198	0.471	16.107%	19.139%	20.199%
L_6	5.751	8.246	0.633	4.235	10.050	0.558	35.793%	17.947%	13.453%
mean	4.711	8.412	0.575	3.860	10.244	0.470	21.891%	17.891%	22.941%

superior to the BEMD-based filter, moreover, the FABEMD-based filter does not have the boundary distortions.

5.4. Comparison with the shearlet-based filter

Take the surface of case study I as an example. The recent developed shearlet-based filter [13] has good filtering performances and is applied to further comparison analysis. The cutoff wavelength of shearlet is 0.64 mm. Table 16 shows the surface amplitude parameters obtained by Gaussian filter and the shearlet-based filter. It can be found from the last three columns in Table 16 that the mean differences are close to 11% in S_a values, close to 9% in S_q values and close to 11% in S_t values. Table 17 shows the surface shape and spacing parameters obtained by Gaussian filter and shearlet-based filter. It can be found from the last three columns in Table 17 that the mean differences are close to 21% in S_{ku}values, close to 18% in S_{al}values and close to 23% in S_{tr}values. The results in Tables 1 and 16 indicate that the FABEMD-based filter and shearlet-based filter have no distinct difference from each other in the surface amplitude parameters. The results in Tables 3 and 17 indicate that the FABEMD filter is better than the shearlet-based filter in the surface shape and spacing parameters. Table 18 shows the differences of the surface amplitude parameters S_a between Gaussian filter and the Shearlet filter, BEMD-based filter and FABEMD-based filter. It can be found that the differences between Gaussian filter and FABEMD-based filter are close to 4.9% in S_a values, which is the smallest. It can also be

Table 18
The comparison of surface amplitude parameters and time using Gaussian filter, shearlet-based filter, BEMD-based filter and FABEMD-based filter.

Unit (um)	Gaussian filter		Shearlet filter		BEMD-based filter		FABEMD-based filter	
	S_a	Difference	Time(s)	Time(s)	Difference	Time(s)	Difference	Time(s)
L_1	0.041	88	12.099%	115	215.208%	412	4.460%	94
L_2	0.049	145	12.500%	121	197.975%	407	4.090%	172
L_3	0.041	93	10.412%	99	199.075%	407	11.965%	96
L_4	0.041	90	11.165%	97	216.821%	546	3.600%	90
L_5	0.042	87	9.953%	106	187.952%	326	1.594%	99
L_6	0.043	89	9.602%	109	192.632%	437	3.809%	95
mean	0.043	98.67	10.955%	129.4	201.610%	422.5	4.920%	107.67

found that the time of FABEMD-based filter is shorter than Shearlet filter and BEMD-based filter, but slightly longer than Gaussian filter

6. Conclusions

In this paper, a novel filter based on FABEMD approach for workpiece surfaces using HDM is proposed. The neighboring window algorithm is presented to extract local extrema and draw the extrema spectrum. The adaptive window algorithm is developed to realize the automatic acquisition of the window size of the order statistics filters. The average smoothing filter is presented for smooth filtering and generating of the mean envelope. The performance of FABEMD-based filter is validated by the simulated surface data and real-world 3D surface data using HDM. Some conclusions can be drawn.

(1) The FABEMD-based filter can effectively decompose the simulated surface into three components: roughness, waviness and form, and has good applicability for workpiece surface filtering.
(2) Compared with the BEMD-based filter, the optimal window width of the order statistic filters searched by the adaptive window algorithm shows its stability and effectiveness, which indicates that the FABEMD-based filter has higher accuracy. The envelope surface in the FABEMD-based filter is drawn by the extremum filters and the average filters, so it has higher efficiency than the BEMD-based filter has. Moreover, the proposed approach does not need to calculate the minimum Euclidean distance between adjacent extreme points and calculate adjacent maxima distance array and adjacent minima distance array.
(3) Compared with Gaussian filter that has obvious distortion at the surface boundary, the FABEMD-based filter has no boundary distortions, and the filtering results are basically same as those of Gaussian filter.
(4) Compared with the shearlet-based filter, the results of the FABEMD-based filter on the surface amplitude parameters are similar, and the results on the surface shape and spacing parameters are better than the shearlet-based filter.

Acknowledgments

The authors greatly acknowledge the editor and the reviewers for their valuable comments and suggestions that have led to a substantial improvement of the paper. This work was supported by the Major Program of the National Natural Science Foundation of China (Grant No. 51535007) and the National Natural Science Foundation of China (Grant No. 51775343).

References

[1] Barari Ahmad. Inspection of the machined surfaces using manufacturing data. J Manuf Syst 2013;32:107–13.
[2] Ramasamy Suresh K, Raja Jayaraman. Performance evaluation of multi-scale data fusion methods for surface metrology domain. J Manuf Syst 2013;32:514–22.
[3] Brinkmann S, Bodschwinna H, Lemke H-W. Accessing roughness in three-dimensions using Gaussian regression filtering. Int J Mach Tools Manuf 2001;41:2153–61.
[4] Krystek M. Form filtering by splines. Measurement 1996;18:9–15.
[5] Goto T, Miyakura J, Umeda K, Kadowaki S, Yanagi K. A robust spline filter on the basis of L2-norm. Precis Eng 2005;29:157–61.
[6] Srinivasan V. Discrete morphological filters for metrology. Proceedings of the 6th ISMQC Symposium on Metrology for Quality Control in Production 1998:623–8.
[7] Raja J, Muralikrishnan B, Fu S. Recent advances in separation of roughness, waviness and form. Precis Eng 2002;26(2):222–35.
[8] Muralikrishnan B, Raja J. Computational surface and roundness metrology. Springer; 2009.
[9] Fu S, Muralikrishnan B, Raja J. Engineering surface analysis with different wavelet bases. J Manuf Sci Eng 2003;125:844–52.
[10] Jiang X, Blunt L, Stout K. Development of a lifting wavelet representation for surface characterization. Proc R Soc Lond Ser A: Math Phys Eng Sci 2000;456:2283–313.
[11] Josso B, Burton DR, Lalor MJ. Frequency normalised wavelet transform for surface roughness analysis and characterization. Wear 2002;252:491–500.
[12] Wang M, Shao Y, Du S, Xi L. A diffusion filter for discontinuous surface measured by high definition metrology. Int J Precis Eng Manuf 2015;16(10):2057–62.
[13] Du S, Liu C, Huang D. A shearlet-based separation method of 3D engineering surface using high definition metrology. Precis Eng 2015;40:55–73.
[14] Huang NE, Shen Z, Long SR, Wu ML, Shih HH, Zheng QN, et al. The empirical mode decomposition and the Hilbert spectrum for nonlinear and non-stationary time series analysis. Proc: Math Phys Eng Sci 1998;454(1971):903–95.
[15] Du S, Liu T, Huang D, Li G. An optimal ensemble empirical mode decomposition method for vibration signal decomposition. J Vib Acoust 2016;139, 031003-1-18.
[16] Flandrin P, Rilling G, Goncalves P. Empirical mode decomposition as a filter bank. IEEE Signal Proces Lett 2004;11(2):112–4.
[17] Wu Zhaohua, Huang Norden E. A study of the characteristics of white noise using the empirical mode decomposition method. Proc: Math Phys Eng Sci 2004;460(2046):1597–611.
[18] Boudraa AO, Cexus JC. EMD-based signal filtering. IEEE Trans Instrum Meas 2007;56(6):2196–202.
[19] Nunes JC, Bouaoune Y, Delechelle E, et al. Image analysis by bidimensional empirical mode decomposition. Image Vis Comput 2003;21(12):1019–26.
[20] Nunes JC, Guyot S, Deléchelle E. Texture analysis based on local analysis of the bidimensional empirical mode decomposition. Mach Vis Appl 2005;16(3):177–88.
[21] Zhou Y, Li H. Adaptive noise reduction method for DSPI fringes based on bi-dimensional ensemble empirical mode decomposition. Opt Express 2011;19(19):18207–15.
[22] Trusiak M, Patorski K, Wielgus M. Adaptive enhancement of optical fringe patterns by selective reconstruction using FABEMD algorithm and Hilbert spiral transform. Opt Express 2012;20(21):23463–79.
[23] (a) Riffi J, Mahraz A, Tairi H. Medical image registration based on fast and adaptive bidimensional empirical mode decomposition. IET Image Process 2013;7(6):567–74;
(b) Bhuiyan SMA, Adhami RR, Khan JF. Fast and adaptive bidimensional empirical mode decomposition using order-statistics filter based envelope estimation. Eurasip J Adv Signal Process 2008;2008(1):1–18.
[24] Bhuiyan SMA, Adhami RR, Khan JF. A novel approach of fast and adaptive bidimensional empirical mode decomposition. IEEE International Conference on Acoustics Speech and Signal Processing. IEEE 2008:1313–6.
[25] Huang Z, Shih A, Ni J. Laser interferometry hologram registration for three-dimensional precision measurements. J Manuf Sci Eng 2006;128, p100613.
[26] Du S, Liu C, Xi L. A selective multiclass support vector machine ensemble classifier for engineering surface classification using high definition metrology. J Manuf Sci Eng 2015;137(1), p011003.

[27] Du S, Huang D, Wang H. An adaptive support vector machine-based workpiece surface classification system using high-definition metrology. IEEE Trans Instrum Meas 2015;64(10):2590–604.
[28] Wang M, Ken T, Du S, Xi L. Tool wear monitoring of wiper inserts in multi-insert face milling using three-dimensional surface form indicators. J Manuf Sci Eng 2015;137(3), p031006.
[29] Wang M, Xi L, Du S. 3D surface form error evaluation using high definition metrology. Precis Eng 2014;38(1):230–6.
[30] Du S, Fei L. Co-Kriging method for form error estimation incorporating condition variable measurements. J Manuf Sci Eng 2016;138(4):p041003.
[31] Huang D, Du S, Li G, Wu Z. A systematic approach for on-line minimizing volume difference of multiple chambers in machining processes based on high definition metrology. J Manuf Sci Eng 2017;139(8), p081003.
[32] Nguyen HT, Wang H, Tai B, Ren J, Hu S, Shih A. High-definition metrology enabled surface variation control by cutting load balancing. J Manuf Sci Eng 2016;138(2), 021010.
[33] Yiping Shao, Shichang Du, Lifeng Xi. 3D machined surface topography forecasting with space-time multioutput support vector regression using high definition metrology. In: Proceedings of the ASME 2017 International Design Engineering Technical Conferences & Computers and Information in Engineering Conference. 2017.